

Magnetic behavior of an amorphous ferromagnet for temperatures close to, and above, the Curie point: Structural relaxation effects

S. N. Kaul* and Ch. V. Mohan

School of Physics, University of Hyderabad, Central University, P.O., Hyderabad 500 134, Andhra Pradesh, India

(Received 19 March 1993; revised manuscript received 23 February 1994)

Detailed bulk magnetization (ac susceptibility) measurements on the amorphous $\text{Fe}_{16}\text{Ni}_{64}\text{B}_{19}\text{Si}$ alloy have been performed in the temperature region $0.95T_C - 1.5T_C$ ($0.95T_C \leq T \leq 1.05T_C$) before and after it had undergone isothermal annealing at 400 K for 60 and 120 min. An elaborate analysis of the data so obtained, besides yielding accurate values for the asymptotic and leading "correction-to-scaling" (CTS) critical exponents and amplitudes, reveals that the structural relaxation consequent upon isothermal annealing does not have any influence on the asymptotic and CTS critical exponents and on the universal amplitude ratios $m_0/M_s(0)$ and Dm_0^8/h_0 , whose values are close to those theoretically predicted for a three-dimensional Heisenberg ferromagnet, but has profound effect on the ratio $\mu_0 h_0/k_B T_C$ and the Curie temperature, T_C . The fraction of spins actually involved in the transition at T_C is small and reduces slowly with increasing annealing time. Consistent with the theoretical expectations, nonanalytic corrections (originating from the nonlinear irrelevant scaling fields) to the singular behavior at T_C dominate over the analytic ones (arising on account of the nonlinear relevant scaling fields) in the critical region but the reverse is true for $T \gg T_C$. Regardless of whether the sample is annealed or not, the initial susceptibility follows the *generalized* Curie-Weiss law for as wide a temperature range as $T_C \leq T \leq 1.5T_C$. The present results provide a strong evidence for weak itinerant ferromagnetism in the glassy alloy in question.

I. INTRODUCTION

The features in the magnetic behavior that distinguish amorphous ferromagnets from their crystalline counterparts are (a) a *steeper*¹ fall in spontaneous magnetization $M_s(T)$ with increasing temperature at low and intermediate temperatures, and (b) a *more* pronounced concave-upward curvature²⁻⁴ in the temperature dependence of inverse initial susceptibility $\chi_0^{-1}(T)$, that persists to much *higher* values of the reduced temperature, $t = T/T_C$ (T_C is the Curie temperature), in the former case. A direct consequence of feature (b) is that the *effective* critical exponent for susceptibility, defined as $\gamma_{\text{eff}}(T) = d[\ln\chi_0^{-1}(\epsilon)]/d(\ln\epsilon)$, where $\epsilon = (T - T_C)/T_C = t - 1$, has roughly the same value⁵ for amorphous and crystalline ferromagnets in the asymptotic critical region $\epsilon \leq \epsilon_{\text{co}}$ (ϵ_{co} is the so-called crossover temperature) but instead of decreasing monotonously^{5,6} towards the mean-field (MF) value for $\epsilon > \epsilon_{\text{co}}$, as in crystalline (ordered) ferromagnets, goes through a peak (peak value, γ_{eff}^p) at ϵ_{max} for amorphous ferromagnets before decreasing towards MF value at $\epsilon \gg \epsilon_{\text{co}}$. The peak in $\gamma_{\text{eff}}(T)$ and its dependence^{5,6} on the concentration of magnetic atoms in a given amorphous alloy system has found *qualitative* interpretation in terms of a number of theoretical⁷⁻¹¹ and phenomenological⁵ models. Considering that the functional dependence of γ_{eff} on temperature for $\epsilon > \epsilon_{\text{co}}$ is markedly different in amorphous and crystalline ferromagnets and that the mean-field calculations,⁷⁻¹¹ on the one hand, and the phenomenological model,⁵ on the other, predict completely different temperature dependence of γ_{eff} in quench-disordered ferromagnets after

they have undergone annealing treatment, a systematic investigation of the influence of structural relaxation (caused by annealing) on $\gamma_{\text{eff}}(T)$ in glassy ferromagnets is expected to provide a rigorous test for the existing theories. These considerations prompted us to perform detailed bulk magnetization and ac susceptibility measurements on an amorphous (*a*-) $\text{Fe}_{16}\text{Ni}_{64}\text{B}_{19}\text{Si}$ sample before and after it had undergone annealing treatment at $T_A = 400$ K for durations of time $t_A = 60$ and 120 min. Another motivating factor for undertaking this type of study was the conflicting reports^{4,12,13} regarding the sensitivity of $\gamma_{\text{eff}}(T)$ to annealing in *a*- $(\text{Fe,Ni})_{80}(\text{B,Si})_{20}$ and *a*- $(\text{Fe,Cr})_{85}\text{B}_{15}$ alloys.

II. EXPERIMENTAL DETAILS

Amorphous (*a*-) ribbons of a cross section 0.04×2 mm² of the alloy with the nominal composition $\text{Fe}_{16}\text{Ni}_{64}\text{B}_{19}\text{Si}$ were prepared by the single-roller melt-quenching technique under high-purity argon atmosphere. The amorphous nature of the ribbons so fabricated was revealed by x-ray diffraction and confirmed by the high-resolution electron microscopic (HREM) technique. Magnetization (M) versus external magnetic field (H_{ex}) isotherms (temperature stability better than ± 40 mK) were measured at ≈ 0.15 K intervals in the temperature range $0.95T_C \leq T \leq 1.05T_C$ and at temperature values ≈ 5 K apart in the interval $1.05T_C < T \leq 1.5T_C$ in fields up to 10 kOe on the *a*- $\text{Fe}_{16}\text{Ni}_{64}\text{B}_{19}\text{Si}$ sample before and after it had undergone isothermal annealing at $T_A = 400$ K for $t_A = 60$ and 120 min. The sample was in the form of a pile of ten ≈ 5 mm-long ribbon strips and its temper-

ature was measured by precalibrated copper-constantan thermocouple. High-precision (relative accuracy better than 10 ppm) ac susceptibility, $\chi_{ac}(T)$, measurements on a single 20-mm-long strip, cut from the same ribbon as that used for the magnetization measurements, before and after it was annealed at $T_A = 400$ K for $t_A = 120$ min, were performed at ≈ 25 -mK intervals in the temperature range $-0.05 \leq \epsilon = (T - T_C)/T_C \leq 0.05$ in a rms ac driving field of $H_{ac} = 100$ mOe and frequency 87 Hz using the mutual inductance method.¹⁴ The sample temperature, monitored by a precalibrated platinum resistance sensor, was kept constant to within ± 10 mK during the measurement period at every fixed temperature setting by a proportional integral and differential temperature controller. $H_{ac}(H_{ex})$ was directed along the length of the strip (strips) within the ribbon plane in $\chi_{ac}(T)[M(H_{ex}, T)]$ measurements to minimize the demagnetization effects. The demagnetizing factor for the samples used in both $\chi_{ac}(T)$ and $M(H_{ex}, T)$ measurements was determined from the low-field (≤ 20 Oe) magnetization data and the measured ac susceptibility as well as H_{ex} were corrected for demagnetization to obtain the intrinsic susceptibility $\chi_0(\epsilon)$ and internal field H , respectively. From a detailed compositional analysis¹⁵⁻¹⁷ and the composition dependence^{3,5,15-18} of T_C in $a\text{-Fe}_x\text{Ni}_{80-x}\text{B}_{19}\text{Si}$ alloys, we infer that the concentration fluctuations in the sample in question could give rise to fluctuations in T_C of the order $\delta T_C \approx 0.1$ K. Therefore, data taken in the reduced temperature range $\leq \delta T_C/T_C$ have been left out of the analysis. The present choice of the annealing temperature is based on the differential scanning calorimetry result that the sample does not get crystallized even when it is annealed at this temperature for two months. This result was further confirmed by the HREM examination. Thus, measurements in the critical region could be performed without any complications due to crystallization.

III. RESULTS AND DATA ANALYSIS

A. Bulk magnetization

The raw magnetization data are converted into the modified Arrott [i.e., $M^{1/\beta}$ versus $(H/M)^{1/\gamma}$] plots through the choice of critical exponents β and γ that makes the $M^{1/\beta}$ vs $(H/M)^{1/\gamma}$ isotherms in a narrow temperature range around T_C straight and parallel to one another over as wide a range of (H/M) values are possible. One such plot, shown in Fig. 1 for the $a\text{-Fe}_{16}\text{Ni}_{64}\text{B}_{19}\text{Si}_1$ alloy in the as-quenched condition, is also representative of those for the annealed samples. Linear extrapolation^{5,12,17} of the high-field straight-line portions of the isotherms to $(H/M)^{1/\gamma} = 0$ and $M^{1/\beta} = 0$ yield intercepts on the $M^{1/\beta}$ and $(H/M)^{1/\gamma}$ axes from which spontaneous magnetization $M_s(T)$ and inverse initial susceptibility $\chi_0^{-1}(T)$ are computed. $M_s(T)[\chi_0^{-1}(T)]$ data so obtained are plotted against $t = T/T_C(T)$ in Figs. 2 and 3; the value of T_C used in Fig. 2 and listed in Tables I and II has been determined by the following method.

Within a narrow temperature range around T_C , $M_s(T)$, and $\chi_0^{-1}(T)$ can be approximated by the single power laws, i.e.,

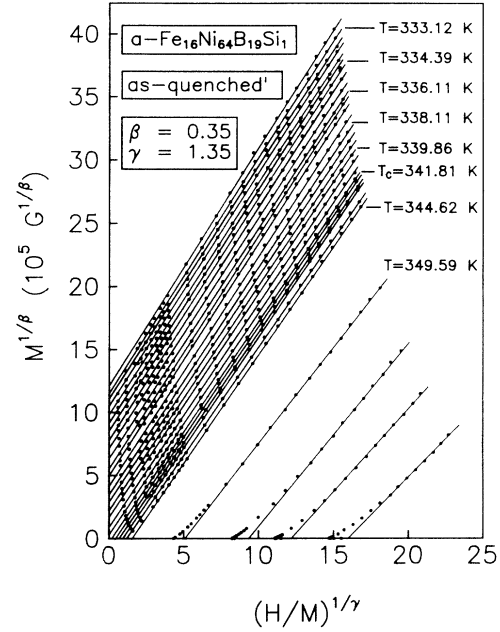


FIG. 1. Modified Arrott plot at a few representative temperatures for the $a\text{-Fe}_{16}\text{Ni}_{64}\text{B}_{19}\text{Si}_1$ alloy in the as-quenched condition.

$$M_s(T) = m_0^{\text{eff}}(-\epsilon)\beta_{\text{eff}}, \quad \epsilon < 0 \quad (1)$$

and

$$\chi_0^{-1}(T) = \Gamma_{\text{eff}}^{-1}\epsilon\gamma_{\text{eff}}, \quad \epsilon > 0. \quad (2)$$

Consequently, the quantities $Y(T)$ and $X(T)$, defined as

$$Y(T) = M_s(T)[dM_s(T)/dT]^{-1} = (T - T_C)/\beta_{\text{eff}}, \quad (3a)$$

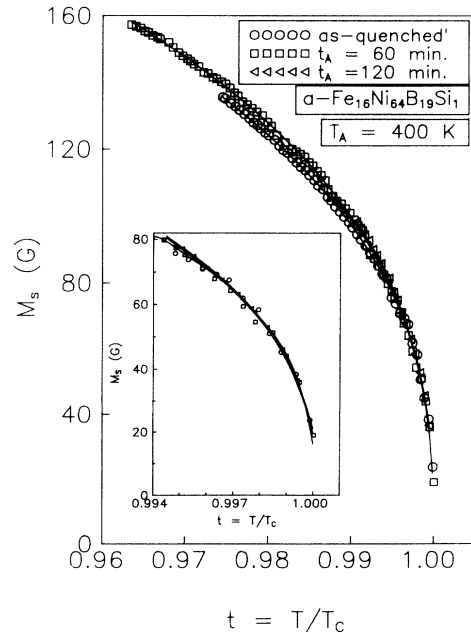


FIG. 2. Spontaneous magnetization as a function of temperature. The continuous curves through the data points represent the best least-squares fits to the data based on Eq. (4) of the text.

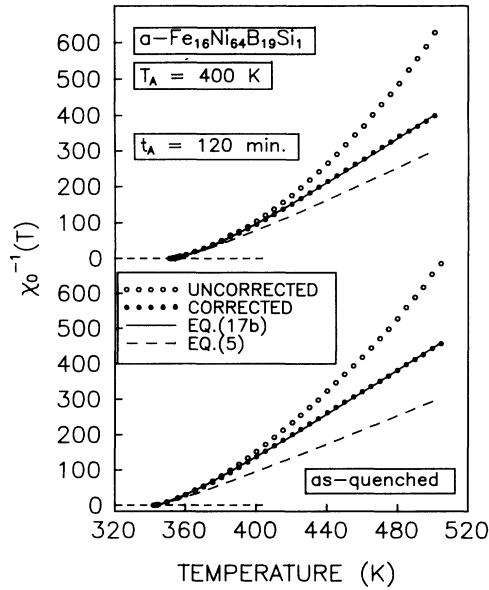


FIG. 3. Temperature variation of the inverse initial susceptibility. The continuous and dashed curves through the corrected data points (solid circles) represent the best least-squares fits to the data in the temperature ranges $T_C \leq T \leq 1.5T_C$ and $T_C \leq T \leq 1.05T_C$, respectively, based on Eqs. (17b) and (5) of the text.

$$X(T) = \chi_0^{-1}(T) [d\chi_0^{-1}(T)/dT]^{-1} = (T - T_C) / \gamma_{\text{eff}}, \quad (3b)$$

when plotted against T should yield straight lines with slopes $(1/\beta_{\text{eff}})$ and $(1/\gamma_{\text{eff}})$, and the intercepts on the T axes equal to T_C . Such plots shown in Fig. 4 demonstrate that this is indeed the case for the glassy alloy in question within the temperature range $-0.02 \leq \epsilon \leq 0.05$. This method, better known as the Kouvel-Fisher (KF) analysis, yields the values for m_0^{eff} , Γ_{eff} , β_{eff} , γ_{eff} , and T_C displayed in Tables I and II; m_0^{eff} and Γ_{eff} are calculated

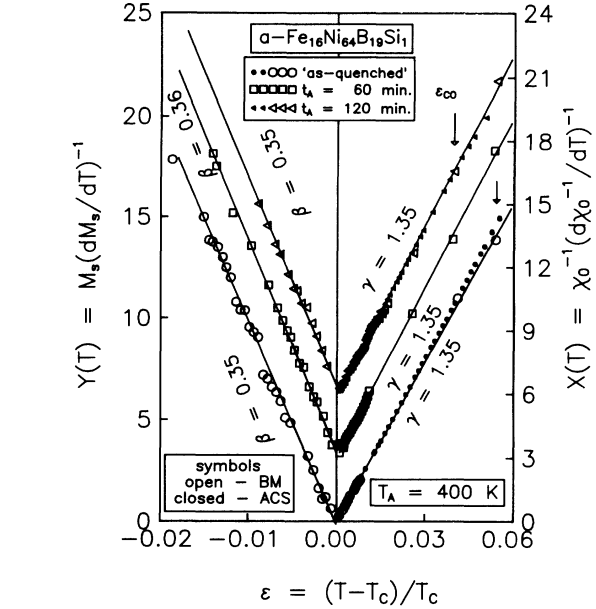


FIG. 4. Temperature dependence of the quantities $X(T)$ and $Y(T)$ in the critical region. ϵ_{co} denotes the temperature beyond which the data deviate from the least-squares fits (straight lines through the data points) based on Eq. (3) of the text. Note that the origin of the ordinate scale for the samples annealed for 60 and 120 min is shifted for the sake of clarity.

from Eqs. (1) and (2) using the KF values of β_{eff} , γ_{eff} , and T_C . Next, the expressions¹⁵ for $M_s(T)$ and $\chi_0^{-1}(T)$ that include the ‘‘correction-to-scaling’’ (CTS) terms, i.e.,

$$M_s(T) = m_0(-\epsilon)^\beta [1 + a_{M_1}(-\epsilon)^{\Delta_1} + a_{M_2}(-\epsilon)^{\Delta_2}], \quad \epsilon < 0 \quad (4)$$

and

$$\chi_0^{-1}(T) = \Gamma \epsilon^{-\gamma} (1 + a_{\chi_1} \epsilon^{\Delta_1} + a_{\chi_2} \epsilon^{\Delta_2}), \quad \epsilon > 0 \quad (5)$$

TABLE I. Asymptotic and leading correction-to-scaling critical exponents and critical amplitudes for spontaneous magnetization as well as critical exponent δ and amplitude D for the critical isotherm of the amorphous $\text{Fe}_{16}\text{Ni}_{64}\text{B}_{19}\text{Si}_1$ alloy before and after it has undergone isothermal annealing. AA—asymptotic analysis (see text), AQ—as-quenched, BM—bulk magnetization, CTS—correction-to-scaling analysis, KF—Kouvel-Fisher analysis, and RG—renormalization group.

t_A (min)	Method	Analysis	Fit range in $10^3\epsilon$	T_C (K)	$[m_0^{\text{eff}}]$ m_0 (emu/g)	$[\beta_{\text{eff}}]$ β	a_{M_1}	a_{M_2}	δ_{obs}	δ_{calc}	D (10^{-3})
AQ	BM	AA-II, KF	0.18–91	341.85(12)	[61.7(9)]	[0.352(10)]					
AQ	BM	AA-II, CTS	0.18–91	341.87(10)	66.2(7)	0.360(5)	-0.056(21)	-0.30(15)			
AQ	BM	$\ln M$ vs $\ln H$		341.81(18)					4.86(10)	4.86(12)	1.354
60	BM	AA-II, KF	0.18–70	351.25(13)	[65.1(4)]	[0.360(10)]					
60	BM	AA-II, CTS	0.18–70	351.27(10)	55.8(10)	0.363(5)	-0.280(30)	0.110(40)			
60	BM	$\ln M$ vs $\ln H$		351.24(18)					5.00(10)	4.83(12)	1.357
120	BM	AA-II, KF	0.04–9	351.24(13)	[62.9(4)]	[0.350(10)]					
120	BM	AA-II, CTS	0.04–9	351.26(10)	53.9(10)	0.362(5)	-0.290(30)	0.100(40)			
120	BM	$\ln M$ vs $\ln H$		351.24(15)					5.00(10)	4.83(12)	1.357
3D- Heisenberg ^a	RG					0.365(3)			4.80(40)		

^aReference 20.

are fitted to the $M_s(T)$ and $\chi_0^{-1}(T)$ data within the same temperature range as above using the nonlinear least-squares-fit computer program that treats m_0 ($\Gamma^{-1}=h_0/m_0$), T_C^- (T_C^+), β (γ), a_{M_1} (a_{χ_1}), and a_{M_2} (a_{χ_2}) as free fitting parameters but keeps the CTS critical exponents Δ_1 and Δ_2 fixed at their theoretically predicted^{16,19,20} values $\Delta_1=0.11$ and $\Delta_2=0.55$. The best theoretical fits (denoted in Figs. 2 and 3 by the continuous and dashed curves, respectively) with the choice of the parameters given in Tables I and II and arrived at in this way (henceforth referred to as the CTS analysis) are *superior* in quality to those (the KF fits) based on Eqs. (1) and (2), as inferred from a considerably reduced value of χ^2 , the sum of deviation squares, for the former type of fits. However, when the $\beta_{\text{eff}}(\epsilon)$ and $\gamma_{\text{eff}}(\epsilon)$ data, computed from the modified versions of Eqs. (3a) and (3b), i.e., $\beta_{\text{eff}}(\epsilon)=[T_C/Y(T)]\epsilon$ and $\gamma_{\text{eff}}(\epsilon)=[T_C/X(T)]\epsilon$, using the KF value for T_C , are compared with the KF fits (dashed lines) and the theoretical values (continuous curves) calculated from the relations¹⁵

$$\beta_{\text{eff}}(\epsilon)=\beta+a_{M_1}\Delta_1(-\epsilon)^{\Delta_1}+a_{M_2}\Delta_2(-\epsilon)^{\Delta_2} \quad (6)$$

and

$$\gamma_{\text{eff}}(\epsilon)=\gamma-a_{\chi_1}\Delta_1\epsilon^{\Delta_1}-a_{\chi_2}\Delta_2\epsilon^{\Delta_2} \quad (7)$$

employing the CTS values (Tables I and II) for $\beta(\gamma)$, a_{M_1} (a_{χ_1}), a_{M_2} (a_{χ_2}), and T_C^- (T_C^+) in Figs. 5 and 6, the improvement in the quality of fits brought about by the inclusion of CTS terms is not (barely) apparent in the case of $\beta_{\text{eff}}(\epsilon)$ [$\gamma_{\text{eff}}(\epsilon)$]. The main reason for this is the *in-*

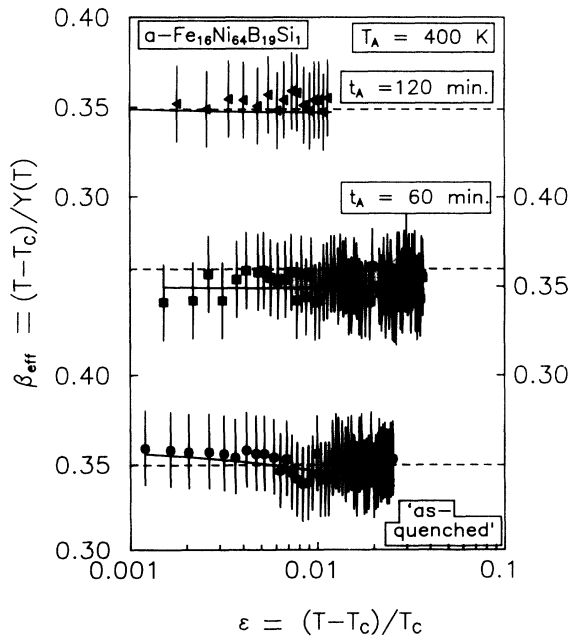


FIG. 5. Variation of the effective critical exponent for spontaneous magnetization, β_{eff} , with temperature. The continuous curves and dashed straight lines through the data points represent the best least-squares fits to the data based on Eqs. (6) and (3a) of the text, respectively.

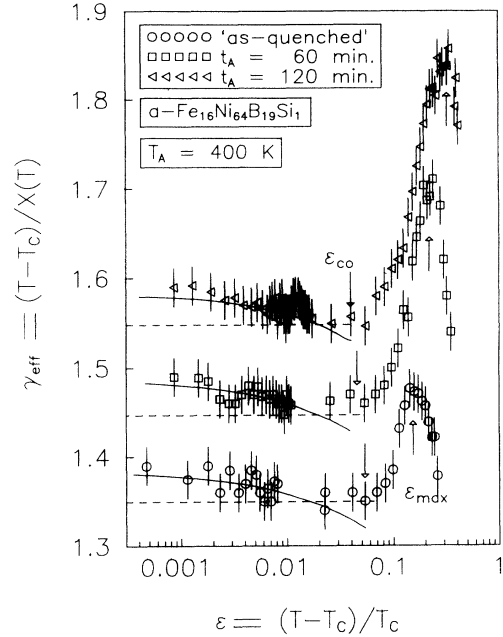


FIG. 6. Variation of the effective critical exponent for initial susceptibility, γ_{eff} , with temperature. The continuous curves and dashed straight lines through the data points represent the best least-squares fits to the data based on Eqs. (7) and (3b) of the text, respectively. Note that the origin of the ordinate scale is shifted up by 0.1 and 0.2 for the samples annealed for 60 and 120 min, respectively, with respect to that for the as-quenched sample.

herent scatter in the $M_s(T)$ [$\chi_0^{-1}(T)$] data, obtained through the above-mentioned extrapolation method, which gets further amplified when the quantity $Y(T)$ [$X(T)$] is computed from such data with a view to arrive at the experimental values of $\beta_{\text{eff}}(\epsilon)$ [$\gamma_{\text{eff}}(\epsilon)$]. Fits to the $M_s(T)$ and $\chi_0^{-1}(T)$ data in the temperature range $0.98T_c \leq T \leq 1.04T_c$ based on the version²¹ of Eqs. (1),

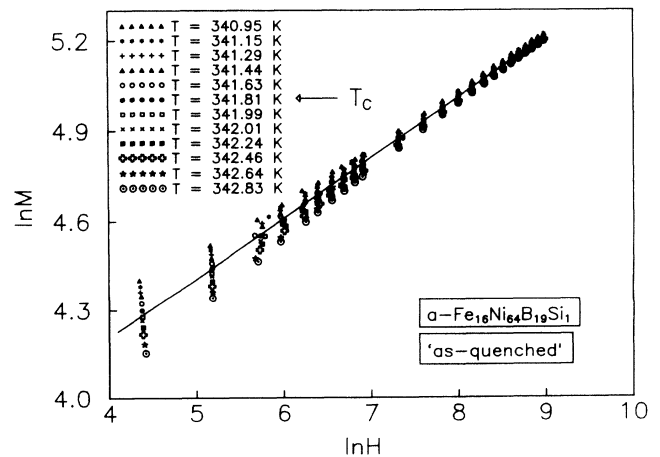


FIG. 7. $\ln M$ vs $\ln H$ isotherms at a few temperatures around the Curie point for the $a\text{-Fe}_{16}\text{Ni}_{64}\text{B}_{19}\text{Si}_1$ sample in the as-quenched condition. The straight line through the data represents the best least-squares fit to the critical isotherm based on Eq. (8) of the text.

(2), (4), and (5) that replaces linear variable ϵ by the nonlinear one, $\tilde{\epsilon} = (T - T_C)/T$, revealed that all the parameters retain their earlier values, i.e., those given in Tables I and II, and practically no improvement in the quality of fits compared to the earlier CTS fits, based on Eqs. (4) and (5), occurs.

The M vs H isotherms measured at temperatures in the range $(T_C - 1 \text{ K}) \leq T \leq (T_C + 1 \text{ K})$ are analyzed in terms of the relation

$$\left. \begin{aligned} M &= A_0 H^{1/\delta} \\ \text{or } H &= DM^\delta \end{aligned} \right\} \epsilon = 0 \quad (8)$$

and the result is shown in Fig. 7. It is noticed that only the $\ln M$ vs $\ln H$ isotherm taken at $T = T_C$ is a straight line with slope δ^{-1} and intercept on the ordinate equal to $\ln A_0$; the isotherms at temperatures on either side of T_C exhibit a finite curvature. The values of T_C , δ , and D (which is related to the critical amplitude A_0 as $D = A_0^{-\delta}$) determined in this way are listed in Table I.

B. ac Susceptibility

Figure 8 displays the temperature dependence of ac susceptibility, corrected for demagnetization, i.e., $\chi_0(\epsilon) = \chi_{\text{meas}}(\epsilon) / [1 - N\chi_{\text{meas}}(\epsilon)]$, where N is the demagnetizing factor, in the critical region $-0.05 \leq \epsilon \leq 0.05$. Increased accuracy (by at least an order of magnitude) of, and substantially reduced scatter in, the ac susceptibility, $\chi_{\text{ac}}(T)$, data compared to the zero-field susceptibility data, obtained through the extrapolation method (Sec. III A), makes $\chi_{\text{ac}}(T)$ data amenable to a more rigorous analysis, whose details have already been reported elsewhere.¹⁵ Therefore, only a brief outline of the steps involved in this analysis are given below. At first, the KF method is used to accurately determine T_C and γ_{eff} from the $X(T)$ vs T plot and then the values of these parameters so obtained (Table II) are inserted in Eq. (2) to compute the corresponding values of Γ_{eff} . Such plots for the

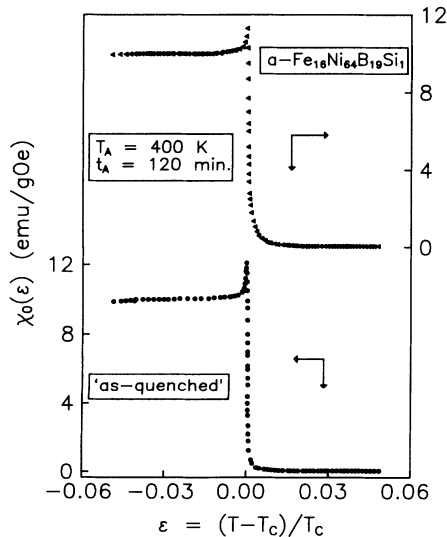


FIG. 8. Temperature dependence of the initial (ac) susceptibility in the range $-0.05 \leq \epsilon \leq 0.05$.

as-quenched and annealed ($T_A = 400 \text{ K}$, $t_A = 120 \text{ min}$) samples, depicted in Fig. 4, demonstrate a *perfect agreement* between the $\chi_{\text{ac}}(T)$ and extrapolated $\chi_0(T)$ data. Next, the values of γ_{eff} at different ϵ , i.e., $\gamma_{\text{eff}}(\epsilon)$, calculated from the relation $\gamma_{\text{eff}}(\epsilon) = [T_C/X(T)]\epsilon$ using $X(T)$ and the KF value of T_C , are used in Eq. (2) to compute $\Gamma_{\text{eff}}(\epsilon)$. Accurate values of γ , Δ_1 , Δ_2 , a_{χ_1} , and a_{χ_2} are obtained by minimizing the mean-square deviation (χ^2) of the theoretical fits, based on Eq. (7), from the $\gamma_{\text{eff}}(\epsilon)$ data with the aid of the nonlinear least-squares-fit computer program which treats γ , a_{χ_1} , and a_{χ_2} as free fitting parameters but varies Δ_1 and Δ_2 in fixed steps of 0.01 within the ranges $0.01 \leq \Delta_1 \leq 0.20$ and $0.35 \leq \Delta_2 \leq 0.75$. The best least-squares fits obtained in this manner are shown in Fig. 9 as continuous curves. The values of γ , Δ_1 , Δ_2 , a_{χ_1} , and a_{χ_2} so determined and listed in Table II are then used in the relation¹⁵

$$\Gamma_{\text{eff}}(\epsilon) = \Gamma(1 + a_{\chi_1}\epsilon^{\Delta_1} + a_{\chi_2}\epsilon^{\Delta_2})\epsilon^{-(a_{\chi_1}\Delta_1\epsilon^{\Delta_1} + a_{\chi_2}\Delta_2\epsilon^{\Delta_2})} \quad (9)$$

to deduce the value of the asymptotic critical amplitude for susceptibility Γ . The values of Γ estimated in this way for the $a\text{-Fe}_{16}\text{Ni}_{64}\text{B}_{19}\text{Si}_1$ sample in the as-quenched condition and after annealing at 400 K for 120 min are also included in Table II for comparison. Consistent with the earlier observation (Sec. III A), the above analysis when repeated for the nonlinear variable $\tilde{\epsilon}$ leaves all the previously determined parameter values (Table II) practically unaltered and brings forth no improvement in the quality of the theoretical fits. Note that the parameter values deduced from the $\chi_{\text{ac}}(T)$ data serve as a crosscheck for those extracted from the extrapolated $\chi_0(T)$ data and a comparison between them sought in Table II asserts that the $\chi_0(T)$ data, when analyzed properly, are capable of yielding accurate values for the parameters Γ , γ , a_{χ_1} , a_{χ_2} , and T_C .

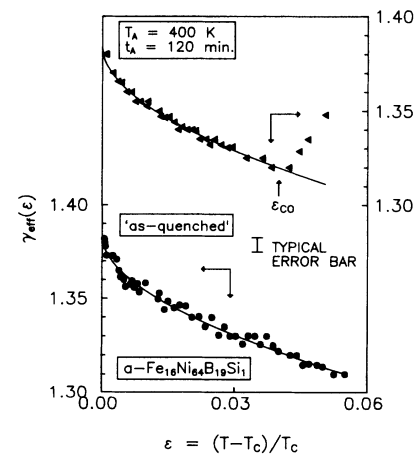


FIG. 9. The effective critical exponent for initial (ac) susceptibility as a function of temperature. The continuous curves through the data points represent the best least-squares fits to the data based on Eq. (7) of the text. ϵ_∞ represents the temperature beyond which the data deviate from the fitted curves.

TABLE II. Asymptotic and leading correction-to-scaling critical exponents and critical amplitudes for the initial susceptibility of the amorphous $\text{Fe}_{16}\text{Ni}_{64}\text{B}_{19}\text{Si}$ alloy before (AQ) and after it has undergone isothermal annealing. AA—asymptotic analysis (see text), ACS—ac susceptibility, AQ—as-quenched, BM—bulk magnetization, CTS—correction-to-scaling analysis, KF—Kouvel-Fisher analysis, and RG—renormalization group.

t_A (min)	Method	Analysis	Fit range in $10^3\epsilon$	T_C (K)	$[\gamma_{\text{eff}}]$ γ	Δ_1	Δ_2	$[\Gamma_{\text{eff}}]$ Γ (10^{-4} emu/g)	a_{χ_1}	a_{χ_2}
AQ	BM	AA-II, KF	0.32–41	341.86(12)	[1.342(30)]			[0.870(40)]		
AQ	BM	AA-II, CTS	0.32–41	341.88(10)	1.388(27)			0.710(70)	0.068(12)	0.58(15)
AQ	ACS	KF	0.40–45	341.87(6)	[1.328(22)]			[0.948(63)]		
AQ	ACS	CTS	0.40–45	341.87(6)	1.386(14)	0.11(4)	0.55(5)	0.750(150)	0.068(12)	0.63(7)
60	BM	AA-II, KF	0.30–39	351.24(12)	[1.350(30)]			[0.844(60)]		
60	BM	AA-II, CTS	0.30–39	351.27(10)	1.390(25)			0.640(100)	0.039(8)	0.63(10)
120	BM	AA-II, KF	0.30–39	351.23(12)	[1.350(30)]			[0.836(60)]		
120	BM	AA-II, CTS	0.30–39	351.26(10)	1.387(23)			0.650(150)	0.033(7)	0.57(11)
120	ACS	KF	0.40–45	351.26(5)	[1.333(17)]			[0.925(40)]		
120	ACS	CTS	0.40–45	351.26(5)	1.386(15)	0.11(3)	0.55(5)	0.660(120)	0.039(4)	0.68(6)
3D- Heisenberg ^a	RG				1.386(4)	0.115(9)	0.550(16)			

^aReference 20.

IV. DISCUSSION

A. Scaling equation of state in linear variables

Tables I–III compare the experimentally determined values of the asymptotic (β, γ, δ) and leading correction-to-scaling (Δ_1, Δ_2) critical exponents and of the universal amplitude ratios with those predicted by the theory^{5,15,19,20} for *isotropic ordered* spin system with *space* (d) as well as *spin* (n) dimensionality of *three*. The main points that emerge from this comparison are (i) the KF and CTS analyses of the $\chi_{\text{ac}}(T)$ and the extrapolated $\chi_0(T)$ data yield identical (within the uncertainty limits) results, (ii) structural relaxation consequent upon isothermal annealing *does not* have any influence on the asymptotic (and leading correction-to-scaling) critical exponents and the amplitude ratios $m_0/M_s(0)$ and Dm_0^δ/h_0 , whereas it appreciably alters the values of *nonuniversal* asymptotic and CTS critical amplitudes (ex-

cept for $\Gamma_{\text{eff}}, \Gamma$, and a_{χ_2}) as well as of the *universal* amplitude ratio $\mu_0 h_0/k_B T_C$ and T_C , (iii) the presently determined values of $\beta, \gamma, \delta, \Delta_1, \Delta_2, m_0/M_s(0)$, and Dm_0^δ/h_0 conform very well with the corresponding theoretical estimates for an isotropic ordered $n=d=3$ spin system with the exception of the ratio $\mu_0 h_0/k_B T_C$, which is lower by at least an order of magnitude, and (iv) the critical exponents β, γ , and δ satisfy the Widom scaling relation $\delta=1+(\gamma/\beta)$ to a high degree of accuracy. While observations (i)–(iii) vindicate the Harris criterion²² and the theoretical predictions,^{23–27} based on the renormalization group (RG) calculations, that the critical behavior of ordered $n=d=3$ spin system with $\alpha < 0$ remains unaltered in the presence of quenched disorder, validity of the Widom scaling relation asserts that the magnetization data taken in the critical region should satisfy the scaling (magnetic) equation of state (SES)

$$m = f_{\pm}(h), \quad (10)$$

TABLE III. Comparison between the experimentally determined and theoretically predicted values for the universal asymptotic amplitude ratios for magnetization. AA—asymptotic analysis (see text), AQ—as-quenched, BM—bulk magnetization, CTS—correction-to-scaling analysis, and KF—Kouvel-Fisher analysis.

t_A (min)	Method	Analysis	$M_B(0)$ (emu/g)	$m_0/M_s(0)$	μ_0 (μ_B)	h_0 (kOe)	$\frac{\mu_0 h_0}{k_B T_C}$ (10^{-2})	Dm_0^δ/h_0	μ_{eff} (μ_B)	c (%)
AQ	BM	AA-II, KF	60.7	1.02(1)	0.528	708.85(49)	7.35	1.35(30)	11.34(20)	4.65(15)
AQ	BM	AA-II, CTS	60.7	1.09(11)	0.528	932.39(18)	9.40	1.35(30)	8.86(20)	5.95(10)
60	BM	AA-II, KF	60.7	1.07(6)	0.528	771.44(27)	7.78	0.95(30)	10.70(20)	4.93(15)
60	BM	AA-II, CTS	60.7	0.92(16)	0.528	869.62(22)	8.78	1.35(30)	9.50(20)	5.55(10)
120	BM	AA-II, KF	60.7	1.04(6)	0.528	751.91(54)	7.59	0.82(30)	10.98(20)	4.80(15)
120	BM	AA-II, CTS	60.7	0.89(16)	0.528	827.30(18)	8.35	1.35(30)	9.98(20)	5.28(10)
3D- Heisenberg ^a				1.37(7)			158.00	1.33(1)		

^aReference 5.

where plus and minus signs refer to temperatures above and below T_C and $m \equiv M/|\epsilon|^\beta$ and $h \equiv H/|\epsilon|^{\beta+\gamma}$ are the scaled magnetization and scaled field, respectively. We, however, prefer to test the magnetization data against an alternate form of SES, i.e.,

$$m^2 = \mp a_{\pm} + b_{\pm}(h/m) \quad (11)$$

for two reasons. First, even the slightest deviations of the data from the universal curves $f_-(h)$ and $f_+(h)$, which escape detection in a $\ln m$ vs $\ln h$ plot because of the insensitive nature of the double-logarithmic scale, are easily discernible² when the same data are plotted in the form of a m^2 vs (h/m) plot; this form of SES, therefore, provides a more rigorous test for the experimentally determined values of the critical exponents and T_C . Secondly, the use of Eq. (11) permits an independent determination of the critical amplitudes $m_0 = a_{\pm}^{1/2}$ and $h_0/m_0 = a_{\pm}/b_{\pm}$ from the intercepts of the universal curves with the m^2 and h/m axes, respectively, in a m^2 vs h/m plot and thereby offers a crosscheck for the amplitude values obtained by the KF and/or CTS analysis. Such m^2 vs h/m plots displayed in Fig. 10, besides demonstrating that the $M(H, T)$ do indeed satisfy Eq. (11), testify to the correctness of the presently determined values of T_C and the exponents β and γ . Moreover, the values of m_0 and (h_0/m_0) computed from the intercepts of the universal curves equal those listed in Tables I and II.

If h_0 is identified with an *effective* exchange interaction field and μ_{eff} is an *average effective* elementary moment participating in the ferromagnetic (FM)–paramagnetic (PM) phase transition, the ratio $\mu_{\text{eff}}h_0/k_B T_C$ is expected to equal the three-dimensional (3D) isotropic nearest-neighbor (nn) Heisenberg estimate of 1.58 because the values of the critical exponents and the remaining amplitude ratios are close to those theoretically predicted for a 3D nn Heisenberg ferromagnet. Evidently, this is not

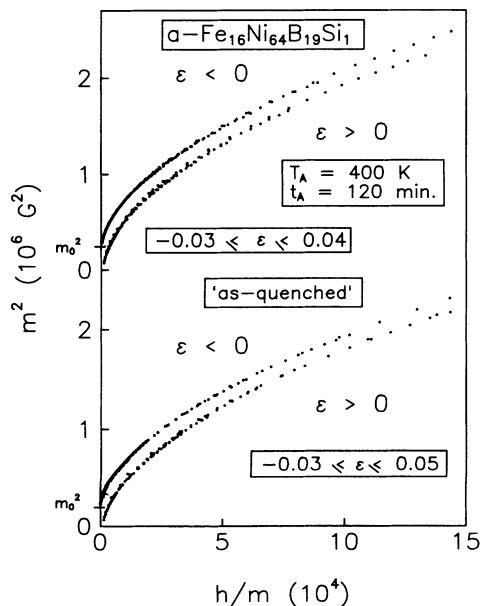


FIG. 10. m^2 vs h/m scaling plots for the as-quenched and annealed samples of $a\text{-Fe}_{16}\text{Ni}_{64}\text{B}_{19}\text{Si}_1$ alloy.

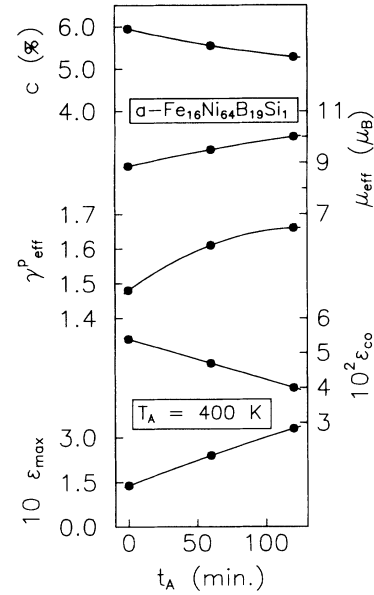


FIG. 11. Variation of the quantities ϵ_{max} , ϵ_{co} , γ_{eff}^p , μ_{eff} , and c with the annealing time t_A .

borne out by the data presented in Table III unless μ_{eff} assumes as high values compared to μ_0 (average magnetic moment per alloy atom at 0 K) as listed in Table III and depicted in Fig. 11. Moreover, the concentration of such effective moments c is given by $c = \mu_0/\mu_{\text{eff}}$. The values of c are also given in Table III. From the variation of c with t_A shown in Fig. 11, it is evident that only about 6% of the moments (i.e., the Fe spins in the present case because Ni atoms in the $a\text{-Fe}_x\text{Ni}_{80-x}\text{B}_{19}\text{Si}_1$ alloy series carry negligibly small¹⁸ moment) actually participates in the FM–PM phase transition in the $a\text{-Fe}_{16}\text{Ni}_{64}\text{B}_{19}\text{Si}_1$ alloy and that this fraction is further reduced as the annealing time t_A is increased. A similar observation²⁸ was previously made by us on $a\text{-Fe}_{100-x}\text{Zr}_x$ alloys.

1. Temperature dependence of the susceptibility effective critical exponent

With reference to the effect of isothermal annealing on $\gamma_{\text{eff}}(T)$ (Figs. 6 and 11) and other relevant magnetic parameters, the important findings that deserve attention are (I) the asymptotic critical exponents β and γ remain unaffected even though the structural relaxation caused by isothermal annealing leads to a substantial *increase* in T_C [$T_C = 341.87$ and 351.27 K for the as-quenched and annealed (for $t_A = 60$ min) samples, respectively]; no discernible change in T_C occurs as t_A increases from 60 to 120 min and a slight *enhancement* in the value of M_s for temperatures well below T_C (Fig. 2), and (II) as t_A increases, (a) the peak in $\gamma_{\text{eff}}(T)$ *broadens*, (b) the peak position, ϵ_{max} , shifts to *higher* temperatures (from $\epsilon_{\text{max}} \approx 1.5 \times 10^{-1}$ for the as-quenched (AQ) sample to $\epsilon_{\text{max}} \approx 3.0 \times 10^{-1}$ for the one annealed for 120 min), while the peak height γ_{eff}^p *increases* from $\gamma_{\text{eff}}^p(\text{AQ}) \approx 1.5$ to $\gamma_{\text{eff}}^p(t_A = 120 \text{ min}) = 1.65$, and (c) the crossover temperature, ϵ_{co} , gets displaced to lower temperatures (from $\epsilon_{\text{co}}(\text{AQ}) \approx 5.5 \times 10^{-2}$ to $\epsilon_{\text{co}}(t_A = 120 \text{ min}) \approx 4.0 \times 10^{-2}$). In

view of the observation that $dT_C/dX \approx 25$ K/at. % Fe in the Fe concentration range of present interest^{3,5,15-18} for α -Fe_XNi_{80-X}B₁₉Si alloys, an increase in T_C of about 10 K as a result of isothermal annealing indicates that after this treatment the alloy in question behaves as if its Fe concentration has increased by nearly 0.4 at. %. In sharp contrast with this interference, the observations II(a)–(c) suggest that the isothermal annealing has the *same effect* on the width of the peak in $\gamma_{\text{eff}}(T)$, ϵ_{max} , γ_{eff}^p and ϵ_{c0} as lowering of Fe concentration in the amorphous alloy series Fe_XNi_{80-X}B₁₉Si has^{5,15,17} on these quantities (see Ref. 5 for details). While the correlated molecular-field theory,^{7,8} the cluster-variational¹⁰ and cluster-expansion¹¹ calculations fail to resolve this contradiction, the Monte Carlo simulations⁹ do offer a simple explanation provided it is conjectured that isothermal annealing increases both the *correlated bond disorder*, which accounts for the observed enhancement of T_C , and *site disorder*, which is responsible for the type of behavior II(a)–(c). However, an increase in both correlated bond and site disorder due to annealing is hard to visualize physically. The only other model, which provides a straightforward explanation for all our observations, is the infinite 3D FM matrix plus finite FM spin clusters model^{5,12,28-30} (henceforth referred to as the FM matrix-FM cluster model), as elucidated below. According to this model, the amorphous alloy under consideration in the as-quenched condition, though *homogeneous* so far as the chemical composition is concerned, contains microscopic regions of low density in an otherwise high-density bulk such that the average nn distance between Fe atoms in these low-density regions (finite-spin clusters) is considerably greater than that in the remaining bulk (infinite FM matrix). As a consequence, the ferromagnetic coupling between spins within the finite clusters is much stronger³⁰ than that between spins in the FM matrix and hence the bulk Curie temperature, T_C , is lower than that for the spin clusters. Due to considerable mismatch in the nn interatomic spacings within the zones that separate these microscopic low-density regions from the high-density bulk, not only large *local quenched-in stresses* but also *strong exchange fluctuations* exist in these zones (for details, see Ref. 30). Hence, the spins within these zones get frustrated through the magnetostrictive mechanism plus the exchange fluctuations. During annealing process, the local quenched-in stresses get progressively relieved through an overall decrease in the average size of the clusters, slight increase in the number of spins in FM matrix at the expense of those originally belonging to the frustration zones, and an increase in the average nn distance between spins in the FM matrix, but soon an optimum arrangement of atoms is reached, which corresponds to a state of system in thermal equilibrium at T_A , such that a further increase in t_A has little or even no effect on both the average size of the finite clusters and the average nn interatomic spacing in the FM matrix. Thus, a steep increase in T_C up to $t_A = 60$ min is followed by saturation at higher annealing times as contrasted with a slight enhancement and early saturation in M_s at low temperatures (increase in M_s is primarily due to a small number of spins, originally belonging to the frustration zones, lost

to the FM matrix during the stress-relief process). The above remarks, however, pertain only to the changes in the low-temperature magnetic behavior brought about by the annealing process and do not take into account the temperature-induced alterations. As $T \rightarrow T_C$, the exchange interaction between the spins in the FM matrix weakens, while the FM coupling between the spins within the finite clusters is still quite strong owing to the higher Curie temperature for the clusters so that the cluster spins polarize an increased number of FM matrix spins and grow in size at the expense of the FM matrix. Therefore, it is not surprising that only a small fraction of spins participates in the FM-PM phase transition and this fraction decreases further with increasing t_A (Fig. 11). Moreover, isothermal annealing promotes temperature-induced cluster growth through the stress-relief process and thereby ensures that by the time temperatures as high as (or just above) T_C are reached the average cluster size has increased as well as the cluster size distribution has broadened as t_A is increased. As a result, isothermal annealing simulates the change in the $\gamma_{\text{eff}}(T)$ peak width, γ_{eff}^p , ϵ_{max} , and ϵ_{c0} normally caused by the magnetic dilution process (the explanation for the effect of magnetic dilution in terms of the FM matrix-FM cluster model can be found in Ref. 5).

B. Scaling equation of state in nonlinear variables

A close examination of the modified Arrott plot (AP) shown in Fig. 1 reveals that the slope of the AP isotherms goes on decreasing with increasing temperature. This feature of the modified Arrott plot is *characteristic*^{5,6} of ferromagnets in the crystalline or amorphous state. The scaling equation of state

$$(H/M)^{1/\gamma} = a_0\epsilon + b_0M^{1/\beta}, \quad (12)$$

that involves the linear variables ϵ and H and forms the basis for the modified Arrott plot, cannot account for the temperature dependence of the slope because the coefficient b_0 (like a_0) is temperature independent. However, within an extremely narrow temperature range around T_C , where the slope of the AP isotherms does not change appreciably, the SES form represented by Eq. (12) is still applicable. Next, the temperature variation of both the slope and intercept, on the ordinate, of the AP isotherms is analyzed in terms of the SES (Ref. 21)

$$M^{1/\beta} = a(-\tilde{\epsilon}) + bt^{-1/\gamma}(H/M)^{1/\gamma} \quad (13)$$

with

$$a \approx \tilde{A}_M [1 + a_{M_1}^- (-\tilde{\epsilon})^{\Delta_1} + a_{M_2}^- (-\tilde{\epsilon})^{\Delta_2}] \quad (14a)$$

or

$$a \approx A_M (1 + a_M^- \tilde{\epsilon}) \quad (14b)$$

and

$$b \approx \tilde{A} (1 + a_1 |\tilde{\epsilon}|^{\Delta_1} + a_2 |\tilde{\epsilon}|^{\Delta_2}) \quad (15a)$$

or

$$b \approx A (1 + \tilde{a}\tilde{\epsilon}) \quad (15b)$$

that makes use of the nonlinear (NL) variables $\tilde{\epsilon} = \epsilon/t$ and $\tilde{h} = H/t$. In Eqs. (14) and (15), (a) and (b) versions of the expressions for the coefficients a and b describe the nonanalytic and analytic corrections to the dominant singular behavior arising from NL irrelevant and relevant scaling fields, respectively. The best least-squares (LS) fits to the observed temperature variation of the slope ($=bt^{-1/\gamma}$) and intercept $\{[M(T,0)]^{1/\beta} = a(-\tilde{\epsilon})\}$ in a narrow temperature range around T_C , based on Eqs. (13)–(15) and obtained by varying the asymptotic and correction amplitudes, while keeping T_C , Δ_1 , and Δ_2 fixed at the KF value, 0.11 and 0.55, respectively, are shown in Figs. 12 and 13 by the continuous (dashed) curves for the version (a) [version (b)] of Eqs. (15) and (14). Such an exercise reveals that (I) inclusion of the correction terms in the expressions for slope and intercept leads to a significant improvement in the quality of the LS fits, (II) the (a) and (b) options of Eqs. (14) and (15) describe equally well the temperature variation of the intercept and slope within the temperature interval $T_C - 5 \text{ K} \leq T \leq T_C + 5 \text{ K}$ (Figs. 12 and 13), and (III) the addition of a constant (which is not predicted by the theory²¹) to Eqs. (15a) and (15b) improves agreement with the experiment considerably (a possible origin of this constant is given below). Success of the nonlinear scaling theory²¹ in correctly predicting the temperature dependence of the slope and intercept encouraged us to attempt a detailed comparison between the observed variation of M_s and χ_0^{-1} with temperature and the one predicted by the expressions given by the nonlinear scaling theory²¹ that either include the leading nonanalytic corrections, i.e.,

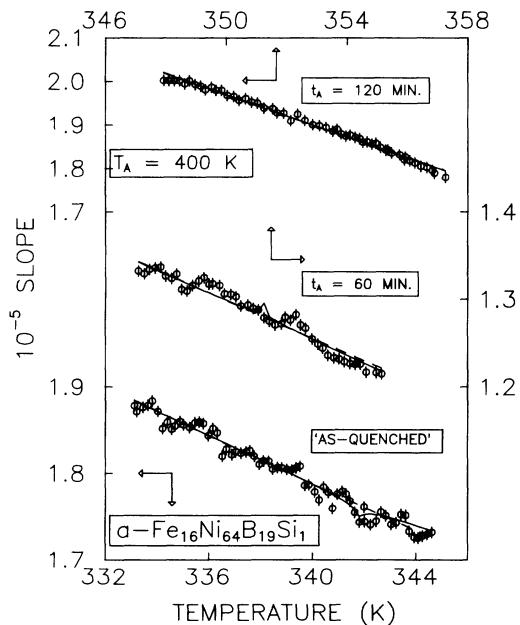


FIG. 12. The slope of the linear Arrott plot isotherms (Fig. 1) as a function of temperature in the critical region. The dashed and solid curves through the data points represent the theoretical variations predicted for the prefactor $bt^{-1/\gamma}$ of the second term in Eq. (13) by Eqs. (15a) and (15b) of the text, respectively.

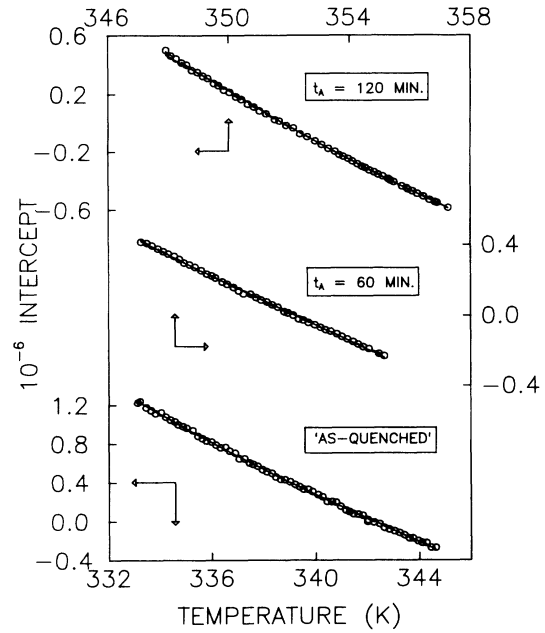


FIG. 13. The intercept $[M(T,0)]^{1/\beta}$ of the linear Arrott plot isotherms (Fig. 1) on the ordinate as a function of temperature in the critical region. The dashed and solid curves through the data points represent the theoretical variations predicted for the term $a(-\tilde{\epsilon})$ in Eq. (13) when a is given by Eqs. (14a) and (14b) of the text, respectively.

$$M_s(T) = m_0(-\tilde{\epsilon})^\beta [1 + a_{M_1}^-(-\tilde{\epsilon})^{\Delta_1} + a_{M_2}^-(-\tilde{\epsilon})^{\Delta_2}], \quad \tilde{\epsilon} < 0 \quad (16a)$$

$$\chi_0(T) = t^{-1} \Gamma \tilde{\epsilon}^{-\gamma} (1 + a_{\chi_1}^+ \tilde{\epsilon}^{\Delta_1} + a_{\chi_2}^+ \tilde{\epsilon}^{\Delta_2}), \quad \tilde{\epsilon} > 0 \quad (16b)$$

or analytic corrections, i.e.,

$$M_s(T) = B_M(-\tilde{\epsilon})^\beta (1 + a_M \tilde{\epsilon}), \quad \tilde{\epsilon} < 0 \quad (17a)$$

$$\chi_0(T) = A_\chi t^{-1} \tilde{\epsilon}^{-\gamma} (1 + a_\chi \tilde{\epsilon}), \quad \tilde{\epsilon} > 0. \quad (17b)$$

The main points that emerge from this comparison are (i) within the temperature ranges $0.96T_C \leq T \leq T_C$ and $T_C \leq T \leq 1.04T_C$ (i.e., in the critical region), Eq. (16a) and Eq. (16b) provide decidedly better LS fits to the $M_s(T)$ and $\chi_0(T)$ data than Eqs. (17a) and (17b); however, in the same temperature range, equally good fits to the $M_s(T)$ or $\chi_0(T)$ data are obtained based on Eqs. (16a) and (4) or Eqs. (16b) and (5), as already mentioned in Sec. III A, and (ii) for³¹ $T \geq 1.29T_C$, the uncorrected $\chi_0(T)$ data (open circles in Fig. 3) are best described by Eq. (17b) plus a constant $B_\chi [= -(7.0 \pm 0.1) \times 10^{-4}$ and $-(9.0 \pm 0.1) \times 10^{-4}$ for the as-quenched and annealed samples, respectively]. In view of the latter finding, $\chi_0(T)$ has been corrected for this additional constant in the entire temperature range $T_C \leq T \leq 515 \text{ K}$ and the LS fits to the resulting (corrected) data (solid circles in Fig. 3) have been attempted using Eqs. (17b) and (16b). It turns out that the LS fits based on Eq. (17b), the continuous curves in

Fig. 3, for $T_C \leq T \leq 1.5T_C$ are far superior in quality to those involving Eq. (16b). Furthermore, the best LS fits based on Eq. (17b) accurately determine the Curie constant $C = A_\chi T_C$, which, in turn, permits a calculation of the effective paramagnetic moment, p_{eff} , through the relation $p_{\text{eff}} = 2.828(CA/\rho)^{1/2}$, where A and ρ are the atomic weight and density, respectively. Regardless of whether the alloy in question has undergone the annealing treatment or not, the ratio of the moment per alloy atom in the PM state, $q_c (= 2.4 \pm 0.1 \mu_B)$, computed from p_{eff} using the relation $p_{\text{eff}}^2 = q_c(q_c + 2)$, to the moment per alloy atom (in the FM state) at 4.2 K, $q_s (= 0.528 \mu_B)$, turns out to be 4.5 ± 0.2 . According to the Rhodes-Wohlfarth criterion,³² such a high value of the q_c/q_s ratio asserts that the investigated glassy alloy is a weak itinerant ferromagnet. This inference is consistent with the conclusions previously drawn from the spontaneous resistivity anisotropy³³ and spin-polarized photoemission³⁴ studies on the same or similar amorphous alloys.

It should be emphasized at this stage that the constant B_χ is too large to be explained either by the presence of higher-order correction terms in Eq. (17b) or in terms of a diamagnetic contribution to $\chi_0(T)$ arising from the electrons in the completely filled shells (and/or Landau contribution from conduction electrons). Since the M vs H isotherms exhibit slight but finite curvature even for temperatures well above T_C presumably due to the presence of finite-spin clusters (short-range magnetic order), we argue that the extrapolation procedure (which gives full weightage to the high-field data only), employed in this work to arrive at the values of initial susceptibility at different temperatures, underestimates $\chi_0(T)$ particularly for $T \gg T_C$ where the magnetization data taken at low fields deviate considerably from the extrapolated straight lines (Fig. 1). Thus, the constant B_χ , in some sense, represents a correction to the extrapolated $\chi_0(T)$ data due to the low-field deviations. We have verified this by comparing the corrected $\chi_0^{-1}(T)$ data with the $\chi_0^{-1}(T)$ values computed from the intercepts of the AP isotherms on the abscissa in Fig. 1 obtained through an extrapolation method that gives equal weightage to the low-field and high-field data. After correcting for B_χ , $\chi_0^{-1}(T)$ loses most of its curvature and exhibits a Curie-Weiss-like behavior (Fig. 3) for $T \geq 1.11T_C$. An immediate consequence of the decreased curvature is that, as the temperature is progressively raised above T_C , the KF effective critical exponent $\gamma_{\text{eff}}^{\text{KF}}(\epsilon)$ [Eq. (3b)] for the corrected $\chi_0(T)$ data stays constant at the 3D-Heisenberg-like value in the range $0 \leq \epsilon \leq 0.15$ and instead of going through a peak, as is the case for the uncorrected data (Fig. 6), gradually decreases from this value for $\epsilon > 0.15$ so as to approach the mean-field (MF) value at $\epsilon \approx 0.5$ (Fig. 14). Such a temperature variation of $\gamma_{\text{eff}}^{\text{KF}}(\epsilon)$ is reminiscent of that usually encountered⁶ in crystalline ferromagnets. Figure 14 also displays the functional dependence on temperature of the effective critical exponents $\gamma_{\text{eff}}^{\text{FS}}(\epsilon)$ [introduced by Fähnle and Souletie³⁵ (FS)] and $\gamma_{\text{eff}}^{\text{NL}}(\epsilon)$, which correspond to the cases²¹ when the coefficient $a_\chi = 0$ and $a_\chi \neq 0$ in Eq. (17b), respectively, and are related to $\gamma_{\text{eff}}^{\text{KF}}(\epsilon)$ through the relations²¹

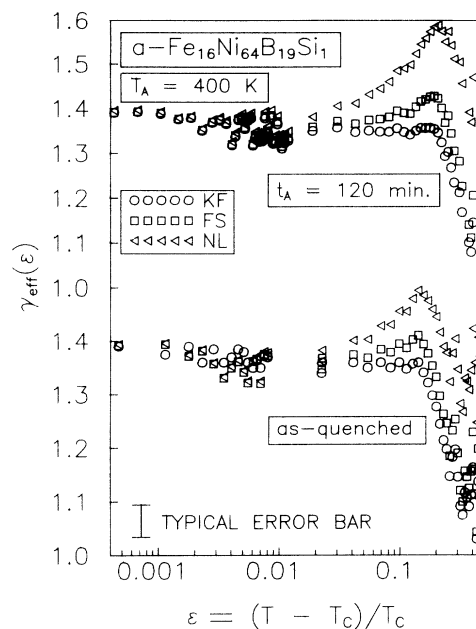


FIG. 14. Temperature variation of the Kouvel-Fisher (KF), Fähnle-Souletie (FS), and nonlinear (NL) forms of the effective critical exponent for the corrected initial susceptibility data.

$$\gamma_{\text{eff}}^{\text{FS}}(T) = \gamma_{\text{eff}}^{\text{KF}}(T) t - \epsilon \quad (18a)$$

and

$$\gamma_{\text{eff}}^{\text{NL}}(T) = \gamma_{\text{eff}}^{\text{FS}}(T) + a_\chi \tilde{\epsilon}, \quad (18b)$$

for the corrected $\chi_0(T)$ data. $\gamma_{\text{eff}}^{\text{FS}}(T)$ for the present alloy, though similar to $\gamma_{\text{eff}}^{\text{KF}}(T)$ and the temperature variation theoretically predicted³⁵ for $S \geq 1$ Heisenberg spins on the fcc lattice, widely differs from the one observed^{36,37} in crystalline ferromagnets in that $\gamma_{\text{eff}}^{\text{FS}}$ in them is either temperature independent³⁶ or increases slightly³⁷ from its asymptotic value over temperatures ranging from T_C to $3T_C$. The finding that in the present case $\gamma_{\text{eff}}^{\text{FS}}(T)$ follows the predictions of the fcc $S \geq 1$ Heisenberg model closely is consistent with the earlier result^{1,2} that the nn atomic configuration in amorphous Ni-rich 3d transition metal-metalloid alloys is fcc-like and $S = 1$ Heisenberg model adequately describes their magnetic behavior. By contrast, $\gamma_{\text{eff}}^{\text{NL}}$, like $\gamma_{\text{eff}}^{\text{FS}}$ in crystalline ferromagnets, is essentially temperature-independent considering large uncertainty in the $\gamma_{\text{eff}}^{\text{NL}}$ values particularly for temperatures $\epsilon \geq 0.1$. The origin of such a large uncertainty in $\gamma_{\text{eff}}^{\text{NL}}(\epsilon)$ can be traced back to the fact that the correction term $a_\chi \tilde{\epsilon}$ in Eq. (17b) [and hence in Eq. (18b)] becomes increasingly important for temperatures $\epsilon > 0.1$ and that the coefficient a_χ could not be determined to an accuracy better than 10% in the present work. In this context, an important point to note is that at the highest temperature (≈ 515 K), the correction term $a_\chi \tilde{\epsilon}$ in Eq. (17b) amounts to 30% (10%) of the asymptotic term for the as-quenched sample (the sample annealed at 400 K for 120 min). Thus, if this decreasing trend in $a_\chi \tilde{\epsilon}$ is maintained as the sample finally goes into the crystalline

state, one would expect this term to be negligibly small for crystalline ferromagnets. In view of Eq. (18b), it is, therefore, not surprising that $\gamma_{\text{eff}}^{\text{FS}}$ is temperature independent for crystalline ferromagnets but not for their amorphous counterparts whereas $\gamma_{\text{eff}}^{\text{NL}}$ has a weak or even no dependence on temperature in the latter case alone.

V. CONCLUSION

The main conclusions, based on the results of the present study, are

(i) In accordance with the Harris criterion and the prediction of the renormalization group calculations that the critical behavior of ordered $n=d=3$ spin system with $\alpha < 0$ remains unaltered in the presence of short-ranged quenched disorder, the asymptotic and leading correction-to-scaling (CTS) critical exponents and the universal amplitude ratios $m_0/M_s(0)$ and Dm_0^δ/h_0 retain their pure values (i.e., those for an isotropic ordered $n=d=3$ spin system) both in the as-quenched and annealed states.

(ii) Structural relaxation consequent upon isothermal annealing does cause substantial change in the values of the asymptotic and CTS critical amplitudes, T_C and the ratio $\mu_0 h_0/k_B T_C$. The fraction of spins that actually participates in the FM-PM phase transition is small and reduces slowly as the sample is annealed for longer durations of time.

(iii) Nonanalytic correction terms, originating from the nonlinear irrelevant scaling fields, dominate over the ana-

lytic ones, arising on account of the nonlinear relevant scaling fields, in the critical region but the reverse is true for $T \gg T_C$.

(iv) Magnetization data obey the equation of state in linear (nonlinear) variables, valid for second-order phase transitions, for temperatures in the immediate vicinity of T_C (in an extremely wide range that embraces the critical region; particularly for $T > T_C$).

(v) Initial susceptibility, $\chi_0(T)$, follows the generalized Curie-Weiss law, Eq. (17b), from T_C to $1.5T_C$ with the 3D Heisenberg-like value for the exponent γ regardless of whether the sample is annealed or not. This permits an unambiguous determination of the atomic moment in the paramagnetic state.

(vi) The alloy in question is a weak itinerant ferromagnet.

(vii) The infinite 3D FM matrix plus finite FM spin clusters model provides a simple qualitative explanation for the temperature dependence of the effective critical exponent, $\gamma_{\text{eff}}(T)$, for susceptibility and for the changes in $\gamma_{\text{eff}}(T)$ brought about by the isothermal annealing.

ACKNOWLEDGMENTS

This work was supported by the Department of Science and Technology, New Delhi, through Grant No. SP/S2/M21/86. One of the authors (Ch.V.M) is grateful to University Grants Commission, New Delhi, for financial assistance.

* Author to whom all the correspondence should be addressed.

¹S. N. Kaul, Phys. Rev. B **27**, 5761 (1983).

²S. N. Kaul, Phys. Rev. B **23**, 1205 (1981); **24**, 6550 (1981).

³S. N. Kaul and M. Rosenberg, Philos. Mag. **44**, 357 (1981); Solid State Commun. **41**, 857 (1982).

⁴K. Zadro, M. Miljak, and H. H. Liebermann, in *Rapidly Quenched Metals*, edited by S. Steeb and H. Warlimont (Elsevier, New York, 1985), p. 1129; P. Hargraves and R. A. Dunlap, J. Phys. F **18**, 553 (1988).

⁵S. N. Kaul, IEEE Trans. Magn. **MAG-20**, 1290 (1984); J. Magn. Magn. Mater. **53**, 5 (1985).

⁶J. S. Kouvel and M. E. Fisher, Phys. Rev. **136**, A1626 (1964); W. U. Kellner, M. Fähnle, H. Kronmüller, and S. N. Kaul, Phys. Status Solidi B **144**, 397 (1987).

⁷M. Fähnle, G. Herzer, H. Kronmüller, R. Meyer, M. Saile, and T. Egami, J. Magn. Magn. Mater. **38**, 240 (1983); M. Fähnle and G. Herzer, *ibid.* **44**, 274 (1984).

⁸T. Kaneyoshi, J. Phys. Soc. Jpn. **51**, 73 (1982); T. Kaneyoshi, I. Tamura, and R. Honmura, Phys. Rev. B **29**, 2769 (1984); T. Kaneyoshi, R. Honmura, I. Tamura, and E. F. Sarmiento, *ibid.* **29**, 5121 (1984).

⁹M. Fähnle, J. Magn. Magn. Mater. **45**, 279 (1984).

¹⁰A. Mitra and S. K. Ghatak, J. Magn. Magn. Mater. **51**, 321 (1985).

¹¹W. Brauneck and D. Wagner, J. Magn. Magn. Mater. **54-57**, 313 (1986).

¹²S. N. Kaul, W. U. Kellner, and H. Kronmüller, Key Eng. Mater. **13-15**, 669 (1987).

¹³U. Gützel and K. Westerholt, Phys. Rev. B **41**, 740 (1990).

¹⁴S. N. Kaul and S. Methfessel, Solid State Commun. **47**, 147

(1983).

¹⁵S. N. Kaul, Phys. Rev. B **38**, 9178 (1988).

¹⁶S. N. Kaul and M. Sambasiva Rao, Phys. Rev. B **43**, 11 240 (1991).

¹⁷S. N. Kaul and M. Sambasiva Rao, J. Phys. Condens. Matter (to be published).

¹⁸S. N. Kaul, IEEE Trans. Magn. **MAG-17**, 1208 (1981).

¹⁹A. Aharony, in *Phase Transitions and Critical Phenomena*, edited by C. Domb and M. S. Green (Academic, New York, 1976), Vol. 6, p. 357.

²⁰J. C. Le Guillou and J. Zinn-Justin, Phys. Rev. B **21**, 3976 (1980).

²¹S. N. Kaul, Phase Trans. **47**, 23 (1994).

²²A. B. Harris, J. Phys. C **7**, 1671 (1974).

²³T. C. Lubensky, Phys. Rev. B **11**, 3573 (1975).

²⁴D. E. Khmel'nitzki, Zh. Eksp. Teor. Fiz. **68**, 1960 (1975) [Sov. Phys. JETP **41**, 981 (1976)].

²⁵G. Grinstein and A. Luther, Phys. Rev. B **13**, 1329 (1976).

²⁶A. Weinrib and B. I. Halperin, Phys. Rev. B **27**, 413 (1983).

²⁷G. Jug, Phys. Rev. B **27**, 609 (1983).

²⁸S. N. Kaul and Ch. V. Mohan, J. Appl. Phys. **71**, 6103 (1992).

²⁹S. N. Kaul and Ch. V. Mohan, J. Appl. Phys. **71**, 6090 (1992).

³⁰S. N. Kaul, J. Phys. Condens. Matter **3**, 4027 (1991); J. Phys. F **18**, 2089 (1988); S. N. Kaul, V. Siruguri, and G. Chandra, Phys. Rev. B **45**, 12 343 (1992).

³¹Now that the analytic corrections to the dominant singular behavior of $\chi_0(T)$ are expected to become important only for temperatures far above T_C , the range-of-fit analysis based on Eq. (17b) in which the variation in the fit parameters A_χ , a_χ , and B_χ is monitored as the temperature range

$T_{\min} \leq T \leq T_{\max}$ is narrowed down by raising $T_{\min} (\gg T_C)$ towards $T_{\max} (=515 \text{ K})$, reveals that these parameters assume constant values only when $T_{\min} \geq 1.29T_C$.

³²E. P. Wohlfarth, *J. Magn. Magn. Mater.* **7**, 113 (1978).

³³S. N. Kaul and M. Rosenberg, *Phys. Rev. B* **27**, 5698 (1983).

³⁴H. Hopster, R. Kurzawa, R. Rane, W. Schmitt, G. Güntherodt, K. H. Walker, and H. J. Güntherodt, *J. Phys. F*

15, L11 (1985).

³⁵M. Fähnle and J. Souletie, *J. Phys. C* **17**, L469 (1984); *Phys. Status Solidi B* **138**, 181 (1986).

³⁶J. Souletie and J. L. Tholence, *Solid State Commun.* **48**, 407 (1983).

³⁷E. Carré, J. P. Renard, and J. Souletie, *J. Magn. Magn. Mater.* **54-57**, 697 (1986).